Perforated exit regions for the reduction of micro-pressure waves from tunnels

Wang, Honglin; Vardy, Alan; Pokrajac, Dubravka

Published in:
Journal of Wind Engineering and Industrial Aerodynamics

DOI:
10.1016/j.jweia.2015.07.015

Publication date:
2015

Document Version
Peer reviewed version

Perforated exit regions for the reduction of micro-pressure waves from tunnels

Honglin Wang[1], Alan E Vardy[2], Dubravka Pokrajac[3]

[1] School of Mechanical Engineering, Southwest Jiaotong University, China
[2] School of Science & Engineering, University of Dundee, UK
[3] School of Engineering, University of Aberdeen, UK

Corresponding author:
Alan VARDY, Research Professor

Address for correspondence:
Dundee Tunnel Research, Kirkton, Abernyte, Perthshire, PH14 9SS, Scotland
E: a.e.vardy@dundee.ac.uk
T: +44 (0) 1828 686 241

Abstract: *The effectiveness of long, perforated exit regions in reducing pressure disturbances from railway tunnels is assessed. Such disturbances always occur, but their amplitudes are usually small. For the particular case of high speed trains, they can reach levels that would cause annoyance in the absence of suitable counter-measures. This risk is especially large in the case of long tunnels. The mechanisms causing the disturbances are described and the potential effectiveness of exit regions as a counter-measure is demonstrated. It is shown that the effectiveness is sensitive to the number, size and distribution of pressure relief holes along the exit region, but that the most important parameter is the combined area of all of the holes. This parameter controls the balance between external disturbances alongside the perforated region and disturbances beyond the exit portal. It is also shown that the amplitudes of the external disturbances are strongly dependent upon the amplitude and duration of wavefronts arriving at the exit region as well as upon their steepness. This contrasts with the behaviour found for tunnels with simple exit portal regions.*

Keywords: *rail tunnel, micro-pressure wave, perforated exit region, pressure gradient, wavefront steepness, counter-measures, sonic boom.*

List of Symbols

c	speed of sound [m/s]
e	total energy per unit volume of air [J/m^3]
F,G	matrices defined in Eq.(1)
H_{slot}	slot height (wall thickness) [m]
L_1	simulated length of tunnel upstream of perforated region [m]
L_{tun}	length of tunnel plus perforated extension [m]
MPW	micro-pressure wave
N_{slot}	number of slots
p	absolute pressure [Pa]
R_G	gas constant [J/kg.K]
R_{tun}	radius of tunnel [m]
r	radial coordinate m]
T	absolute temperature [K]
t	time coordinate [s]
u,v	velocity components in x,r directions [m/s]

U,W	matrices defined in Eq.(1)
W_{slot}	width of roof slot [m]
X_{slot}	distance between slot centres [m]
x	axial coordinate [m]
Y_{ref}	distance between MPW reference line and nearest part of tunnel [m]

Greek characters

ρ	air density [kg/m^3]
γ	ratio of principal specific heat capacities [-]

1 Introduction

The radiation of micro-pressure waves (MPWs) from railway tunnels has received close attention since the first bullet trains in Japan [Ozawa *et al* 1991; Ozawa 1992]. These pressure disturbances are much smaller than pressure waves inside tunnels, but they can annoy people who are not using the railway itself. The most likely sources of annoyance arise from low frequency components of MPWs. These can excite structural features that are sensitive to vibration, notably doors and windows of nearby buildings. In rare cases, higher frequency components in the audible range can occur and are loosely referred to as "sonic booms". The disturbances were first detected during commissioning trials on the early Shinkansen network and some examples were quite strong [Ozawa & Maeda 1988; Ozawa *et al* 1993; Matsubayashi *et al* 2000]. However, remedial measures were soon implemented and it is unlikely that strong examples will occur anywhere in future – because designers are now aware of the phenomenon.

Understanding of the underlying physics of the phenomenon is good, but the ability to predict the likely amplitudes of MPWs accurately is less good. This is because there is a strong dependence on the amplitude-frequency characteristics of internal wavefronts that cause them when reflecting at a tunnel portal. In all tunnels, these depend strongly on the detailed shapes of train noses and tunnel entrances. In long tunnels, they also depend strongly on the nature of the tunnel lining and on fixtures and fittings along the tunnel. Another big complication is that, even if the predictive ability were excellent, an important hurdle would remain, namely identifying suitable acceptability criteria for MPWs. As with most noise-related phenomena, this is a subjective matter that cannot be addressed satisfactorily by technical analysis alone. Criteria that are appropriate for a tunnel in one location might not be suitable for a tunnel in another location. For generic design purposes, the most common approach is somewhat pragmatic, with comparisons between alternative designs being made on the basis of a single-valued criterion, namely the maximum amplitude of the MPW, regardless of its frequency distribution. In these cases, a standard reference location is usually chosen, typically 20 m or 25 m from the centroid of the plane of the relevant tunnel portal and, perhaps, at an angle of 45° to the plane [Ravn & Reinke 2006; Degen *et al* 2008; Gerbig & Degen 2012; Hieke *et al* 2011]. More detailed, frequency-dependent, criteria are coming into use for the assessment of measured pressures and these can be chosen to suit the site-specific usage of the region close to the any particular tunnel [Degen *et al* 2008; Gerbig & Degen 2012; Hieke *et al* 2011].

MPWs are created whenever a pressure wave reflects at an open end of a duct. In a dominant majority of cases, however, their amplitudes are far below levels likely to cause nuisance. Possible exceptions include, for example, guns and vehicle exhausts as well as railway tunnels, but only the latter are considered herein. In part, this is because of the special geometrical configurations of each possible application and, in part, it is because of the widely different frequency-amplitude

characteristics in the different applications. This, together with practical constraints, has a major influence on the nature of potentially useful remedial measures. In the case of railway tunnels, by far the most common method of reducing MPWs radiating from tunnel *exit* portals is the construction of special extension regions at *entrance* portals. This highly effective counter-measure is logical because (i) the amplitudes of MPWs depend strongly on the steepness of pressure waves approaching the exit portal, (ii) the particular case that is most commonly troublesome is a wavefront generated during train-entry to a tunnel and (iii) it is relatively easy to design entrance regions that will ensure that nose-entry wavefronts do not exceed an acceptable steepness.

The use of special entrance regions to combat MPW development becomes questionable in the case of long tunnels – for two key reasons. First, the nose-entry wavefront is a compression wave and so, in slab-track tunnels that are popular in today's high-speed railways, it steepens as it propagates [Mashimo *et al* 1997, Fukuda *et al* 2006, Miyachi *et al* 2008]. The required entrance length to compensate for this effect can become excessive - over 200 m in some (unpublished) cases. Second, long tunnels often have shafts for ventilation, pressure relief or access and these are additional sources of wavefronts when trains cross them. Extended entrance regions have no influence whatsoever on these internally-generated waves and it would rarely be practicable to provide equivalent extended regions at such locations. Possible ways of countering wavefront steepening during propagation can be envisaged, but the most obvious response is to explore the possibility of providing remedial measures at the exit portal itself. Measures at this location have the potential to be effective for all incident wavefronts, irrespective of their origins.

The literature includes papers describing a range of exit alleviation possibilities. These range from passive devices involving large chambers that are loosely reminiscent of vehicle exhaust silencers/mufflers [Aoki *et al* 1999; Sockel & Pesave 2006; Kim *et al* 2004; Raghunathan *et al* 2002] to active devices that create a tailored response to the specific characteristics of each incident wavefront. Active devices utilise the concept of "anti-noise" in one form or another [Raghunathan *et al* 2002; Vardy 2008; Matsubayashi *et al* 2004]. They have the strong theoretical advantage of being potentially highly effective and yet compact, but also the disadvantages of being reliant on the reliable availability of power and potentially being capable of exacerbating the situation in the event of malfunction. Herein, attention focusses on a *passive* measure, namely the provision of long, perforated extensions at exit portals (Fig-1). These have a special advantage over many other counter-measures, namely that they might also provide benefit as extended *entrance* regions when trains travel in the opposite direction. This is relevant even in single-track tunnels because railway operators commonly require the capability of operating at full design speed in either direction even if such capability is intended only for back-up purposes.

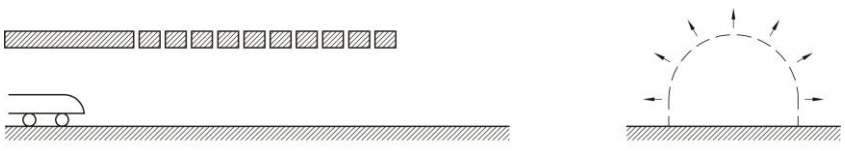

(a) Longitudinal geometry (b) Indicative cross-section

Fig-1 Indicative geometries for perforated exit regions

The remainder of this paper begins with a brief outline of the theoretical methodology and a summary of the physical behaviour expected in the absence of remedial measures. Then, the performance of a base-case perforated extension is considered, including an assessment of the

dependence of such regions on the dominant characteristics of incident wavefronts (amplitude and steepness). Thereafter, the focus is on the effectiveness of alternative configurations of the perforated region – namely its size and the distribution of holes in its walls. Finally, conclusions of relevance to practical design are presented.

2 Theoretical approach

The detailed performance of any particular exit region will depend upon the geometrical configuration of the region and also on that of the tunnel and on the external topography. For the present generic investigation, the chosen geometry is as illustrated in Fig-1(a)&(b). It is loosely representative of a tunnel emerging into open ground and it approximates to an axi-symmetric configuration. Accordingly, an axi-symmetric geometry is assumed in the theoretical development, thereby greatly reducing computational demands in comparison with fully 3-D simulations without significantly downgrading the usefulness of the predictions. Strictly, the use of axi-symmetric geometry carries an improbable implication that holes in the wall of the perforated region extend around the whole of the circumference. However, the total area of such holes will be more important than their detailed circumferential distribution except close to the wall.

Another simplification that yields big advantages with only small adverse implications for applicability is the use of inviscid analysis. In the real case, the air flows will be turbulent, but the flow Reynolds numbers will be so high that inertia forces will be dominant over most of the flow domain during the timescales of interest [Ofengeim and Drikakis 1997]. The only important exception to this rule will be local contractions in flow as air passes through the holes/slots in the wall. Even in these locations, however, the adverse consequences of the simplification will be small if the holes are reasonably streamlined (i.e. if they have suitably curved edges). As a consequence, it is reasonable to utilise axi-symmetric Euler equations [Aoki *et al* 1999], namely:

$$\frac{\partial \mathbf{U}}{\partial t}+\frac{\partial \mathbf{F}}{\partial x}+\frac{\partial \mathbf{G}}{\partial r}+\mathbf{W}=0 \tag{1}$$

in which

$$\mathbf{U}=\begin{bmatrix}\rho\\ \rho u\\ \rho v\\ \rho e\end{bmatrix} \quad \mathbf{F}=\begin{bmatrix}\rho u\\ \rho u^2+p\\ \rho uv\\ (\rho e+p)u\end{bmatrix} \quad \mathbf{G}=\begin{bmatrix}\rho v\\ \rho uv\\ \rho v^2+p\\ (\rho e+p)v\end{bmatrix} \quad \mathbf{W}=\frac{1}{r}\begin{bmatrix}\rho v\\ \rho uv\\ \rho v^2\\ (\rho e+p)v\end{bmatrix}$$

In this equation, x and r denote the axial and radial coordinates, t is the time coordinate, u and v are velocity components in the x and r directions, and ρ and p are the air density and absolute pressure. The total energy per unit volume of air, e, is the sum of the kinetic and internal energies, namely:

$$e=\frac{p}{\rho(\gamma-1)}+\frac{u^2+v^2}{2} \tag{2}$$

in which γ denotes the ratio of the principal specific heat capacities of the air. The equations are closed by regarding the air as a perfect gas satisfying the equation of state:

$$p = \rho R_G T \tag{3}$$

where R_G is the gas constant for air and T is the absolute temperature.

2.1 Solution method and validation

The simulation domain is shown in Fig-2(a). It includes a short region of tunnel leading to the perforated exit region. At the upstream boundary inside the tunnel, the pressure is prescribed to increase linearly from the ambient pressure to a predetermined value at which it is then held constant. This is an idealised form of many possible shapes of wavefront that could propagate along a tunnel towards its outlet portal. The simplified form of the prescribed wavefront facilitates assessments of the influence of the most important characteristics of incident wavefronts.

The numerical solutions presented below are based on axi-symmetric approximations, thereby implying that the slots are continuous over the whole of the circumference. In practical construction, however, it is much more likely that discrete holes would be formed in the manner indicated in Fig-2(b). To achieve the same overall slot area, the decreased circumferential extent of the slots would necessitate a corresponding increase in their lateral dimensions. For the physical phenomenon under consideration, the overall slot area is far more important than the detailed shapes of the openings so this simplification is of little practical consequence.

Beyond the tunnel, the simulation domain extends up to a remote null reflection boundary shown in Fig-2(a). Since it is not possible to achieve wholly non-reflecting conditions for waves propagating in a 2-D or 3-D manner, this boundary is placed sufficiently far beyond the outer portal to have negligible influence during the timescales reported in the predicted results. All other boundaries in the simulation are at solid surfaces over which the (inviscid) fluid slides with no resistance, i.e. they are specified as free-slip boundaries.

Initially, the pressure and (zero) velocity are uniform over the whole domain. All subsequent variations are consequences of the prescribed pressure variation at the upstream tunnel boundary.

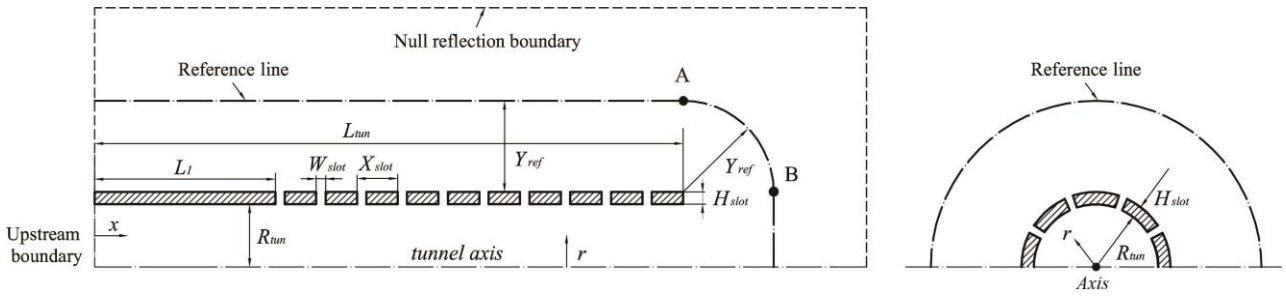

Fig-2 Tunnel geometry and solution domain
(*The Reference line is explained in Section 3. It defines the location at which graphical results are presented outside the tunnel*)

Numerous advanced numerical schemes for simulating wave propagation have been proposed in the literature, e.g. [Zoltak and Drikakis 1998, Toro 2001, Leveque 2002]. Specialised methods exist for a wide range of flow types (e.g. shocks), but the use of such methods is not necessary for

geometrical configurations and pressure waves of the steepness considered herein. This is because it is possible to achieve high accuracy using standard numerical schemes already implemented in widely available commercial software, provided that appropriate attention is paid to the design of the numerical grids and to the application of suitable numerical checking processes. The particular software used herein is ANSYS FLUENT [26], with the following options: density-based solver, Roe-FDS Flux Scheme, third-order MUSCL for spatial discretization and 2nd-order implicit time stepping for temporal discretization. To achieve good accuracy in a numerical simulation, careful attention has to be paid to the design of the numerical grids and to the application of suitable validation processes. In the present case, the modelling capability of the selected solver and the choice of the grid size and time step have been validated in two stages.

One stage concerned the choice of the spatial sizes of the grid elements, which need to be sufficiently small to enable the predicted flow to respond to all relevant geometrical details. For simulations presented herein, a grid size of $R_{tun}/50 = 0.1$ m is used over the whole of the solution domain inside the tunnel and close to the tunnel. An increased grid size is used in the far field where pressure wave amplitudes are much smaller than in the near field and where rates of change are even smaller. The chosen grid would be too coarse to reproduce detailed flow structures close to the corners of the slots (indeed, no grid could achieve this exactly for the assumed inviscid flow), but it is more than adequate for simulating wave propagation through the slots. This is because the time scales associated with wave propagation across the slots are small in comparison with scales of practical relevance to the resulting MPWs. The selected grid sizes have been validated by performing a grid-independence study which involved progressive refinement of the grid sizes by factors of 2. In a previous study, Wang *et al* [2015, Fig-6] showed that predictions obtained with double the spatial steps used herein were very close indeed to those obtained with this smaller grid. That is, the grid size used in the present study yields almost grid-independent predictions, with a safety margin of two in comparison with a grid size that would be almost equally acceptable. The comparisons for which this assessment was made include time series predictions of pressure at ground level outside the tunnel portal and mass flow rates through the slots.

The other stage involved choosing a numerical time step of integration appropriate for the detailed analysis of wave propagation. This implies a need for time steps that are smaller than the time needed for a wave to travel one spatial grid length, usually expressed through a Courant number (=the ratio between (i) the distance travelled by a wave during a single time step and (ii) the spatial grid size). In the present study, the time step was 0.1 ms, corresponding to a Courant number of approximately 0.34 with a grid size of 0.1 m and a sound speed of approximately 340 m/s. It is not possible to achieve the same Courant number everywhere, partly because waves travel simultaneously in all directions whereas numerical grids are inevitably direction-dependent, and partly because of the use of different spatial grid sizes in different locations (to avoid unnecessary detail in regions far from the portal). However, it *is* possible to confirm the suitability of the chosen time steps. This has been done by simulating a test case with waves exhibiting non-linear steepening that can be predicted analytically. A detailed comparison between the numerical simulation and a quasi-analytical solution based on a plane-wave behaviour is given by Wang *et al* [2015, Fig_5]. It shows that a numerical simulation with computational parameters similar to those used in the present study is able to predict wave steepening behaviour along a tunnel with good accuracy, even in the extreme case where the wavefront is close to becoming a shock. The close agreement obtained for this non-linear effect in the presence of rates of change of pressure far exceeding those in the present application is a strong indication of the suitability of the chosen grids.

3 Exit region without slots

It is instructive to preface the assessment of perforated exit regions by a description of how a pressure wave inside a tunnel can cause MPWs outside the tunnel even though the amplitude of the wavefront reflected back along the tunnel is almost the same as that of the incident wavefront. The flow process that causes this behaviour is illustrated schematically in Fig-3(a)&(b). In Fig-3(a), a short, plane wavefront is shown approaching a portal. It could be either an isolated wavefront or one of many small wavefronts that collectively comprise a larger one. Its plane-wave character, which is typical of waves that have travelled along uni-directional ducts, is such that similar conditions exist at all radii in the cross-section. However, this state cannot persist after the wavefront has reached the portal plane. From that instant, the possibility of radial expansion exists and the wavefront responds to this. At timescales relevant to waves, it does this in all directions simultaneously, as illustrated in Fig-3(b). Eventually (i.e. after the short time R_{tun}/c where R_{tun} denotes the tunnel radius and c is the speed of sound), the whole of the cross-section will have been influenced by the radial expansion, albeit to different extents at different radii. Until this instant, however, the part of the incident wavefront closest to the central axis will have continued as before and, as a consequence, some high pressure air will have passed from the tunnel into the surroundings. This is the leading part of the MPW. It is of interest to note in passing that this mechanism also contributes to the projection of "smoke-rings" from the end of a duct – although that effect is additionally dependent on factors that are not included in the present analysis. Figure-3(c) shows a loosely analogous behaviour when a wavefront passes an open slot in a wall; this case is studied in detail later in the paper.

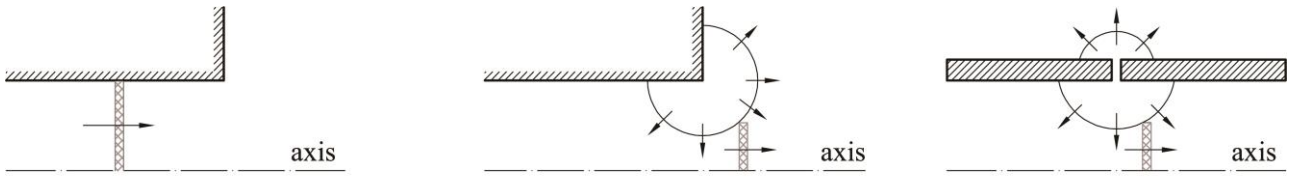

(a) (b) (c)

Fig-3 Indicative influence of 2-D/3-D geometry on plane wave propagation
(a) Plane wave approaching an exit portal
(b) Reflection/transmission at an exit portal
(c) Reflection/transmission at a wall slot

Figure-4 shows gauge-pressure profiles along the tunnel axis before and after an incident wavefront reaches the exit portal. For clarity, the profiles are shown in two periods. In Fig-4(a), which shows the period until shortly after the toe of the wavefront reaches the portal plane, the incident wavefront is travelling from left to right and its shape remains almost unchanged. Thereafter, as illustrated In Fig-4(b), the reflection/transmission process causes a reflected wavefront to propagate back upstream and it also causes an MPW to propagate into the surrounding medium. During the main period of reflection, the steepness of the reflected wavefront is similar to that of the incident wavefront, but the early and later stages of the reflection cause more gradual changes. This is especially noticeable in the later stages during which the gauge pressure approaches zero asymptotically. Note that, in the remainder of the paper, the "gauge pressure" is referred to simply as "pressure". This is consistent with a widely-followed, unwritten convention in wave mechanics. In studies of acoustics, for instance,

the term “acoustic pressure” is commonly abbreviated to “pressure” provided that the true meaning is obvious from the context.

Outside the tunnel, the pressure varies in a pulse-like manner, initially increasing and then decreasing. The pulse propagates radially outwards, reducing in amplitude as it does so. This pulse is the MPW. It is more complex than this description of a simple rise and fall and, furthermore, its amplitude varies with orientation relative to the tunnel axis. For practical design purposes, however, its primary component is usually regarded approximately as a spherical pulse, except in a transition zone in which the wavefront changes from predominantly uniaxial to predominantly spherical.

Figure-4(c) shows pressure distributions along a reference line that is everywhere a distance Y_{ref} from the nearest location on the outer surface of the tunnel (or the portal plane), as shown in Fig-2. A comparison of Figs-4(b) and 4(c) shows that the part of the pulse that is travelling back along the outside of the tunnel is almost coincident with the reflected pulse travelling back along the inside of the tunnel. However, the amplitude of the former reduces approximately inversely with distance from the portal whereas the amplitude of the internal reflection does not change as it propagates. The different generic behaviours exist because the pulse outside the tunnel is expanding spherically whereas the internal flows are almost uniaxial.

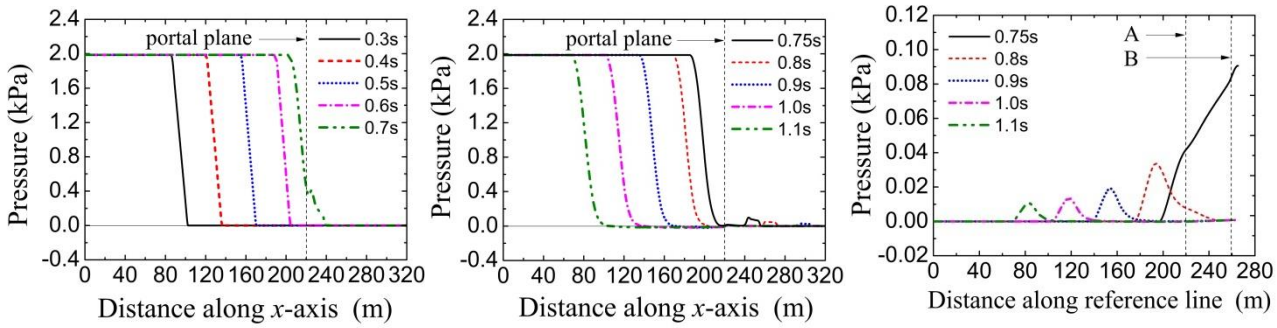

(a) (b) (c)

Fig-4 Pressure profiles along an unperforated exit region (R_{tun}=5m)
(a) Wavefront approach
(b) Reflection/transmission at portal
(c) Pressure along the reference line (The points A & B are defined in Fig.2)

4 Exit region with slots

Attention now turns to the case of a perforated exit region. In this Section, all simulations refer to a particular geometry and the focus is on the dependence of the flow behaviour on the major characteristics of the incident wavefront. The general form of the region is as depicted in Fig-2 and the particular dimensions are listed in Table-1.

Table 1 Dimensions of the perforated exit region

Dimension	Value	Description
L_1	120 m	Length of tunnel to start of perforated extension
L_{tun}	220 m	Length of tunnel to end of perforated extension
R_{tun}	5 m	Radius of tunnel

W_{slot}	0.4m	Width of slots
X_{slot}	10 m	Distance between slot centres
H_{slot}	1 m	Length of slots (wall thickness)
N_{slot}	10	Number of slots
Y_{ref}	25 m	Distance of reference line from outer surface

Figure-5 shows longitudinal pressure profiles after the arrival of an incident wavefront identical to that assumed in Fig-4 for an unperforated exit region. At the first instant shown in Fig-5(a), the toe of the incident wavefront has not yet reached the beginning of the perforated region (120 m). The figure shows subsequent pressure profiles until shortly after the toe has reached the exit portal plane. There are two major differences from the corresponding profiles in Fig-4(a) for an unperforated tunnel. First, the primary wavefront attenuates strongly as it propagates along the exit region. Second, strong reflections propagate upstream in the tunnel long before the wavefront reaches the portal. Both of these effects are easily foreseen consequences of the continual leakage of mass through the slots in the tunnel wall. So are pressure changes outside the tunnel as a consequence of the lateral leakage, as illustrated in Fig-5(b) along the reference line.

In contrast with the unperforated tunnel case, waves cannot propagate in a plane-wave manner along the perforated region. This is an inevitable consequence of the leakage being localised in the cross-section (i.e. at the tunnel wall). As illustrated in Fig-3(c), the direct influence of any particular slot is local and its influence at all other locations is dependent upon the time required for waves to reach those locations. This is especially important close to the axis of the tunnel where, as seen in Fig-5(a), a short pulse-like zone develops close to the axis at the toe of the wavefront. This behaviour is important because it significantly reduces the benefit that is realised from the huge reduction caused by the slots on the overall steepness of the wavefront.

Attention is drawn to the development of negative (gauge) pressures in the leading parts of the wavefront. At first sight, this may be unexpected, but it is open to a simple interpretation. To pursue this, it is instructive to digress slightly by considering a negative wavefront propagating towards the closed end of a pipe. On arrival at the closed end, such a wavefront will reflect and its negative amplitude will double. Now consider a negative wavefront propagating radially inwards from a slot in the perforated region of tunnel. This wavefront will be moving into an increasingly "closed" region (because it is propagating towards $r = 0$). Accordingly, its amplitude will tend to increase. Of course, the full picture is more complex that this simple analogy implies (e.g. the wavefront will spread axially as well as radially). Nevertheless, this is an important part of the cause of the negative pressures. For completeness, however, it has been confirmed formally that the effect is physical, not spurious. This has been done by comparing detailed simulations with successively reduced grid sizes.

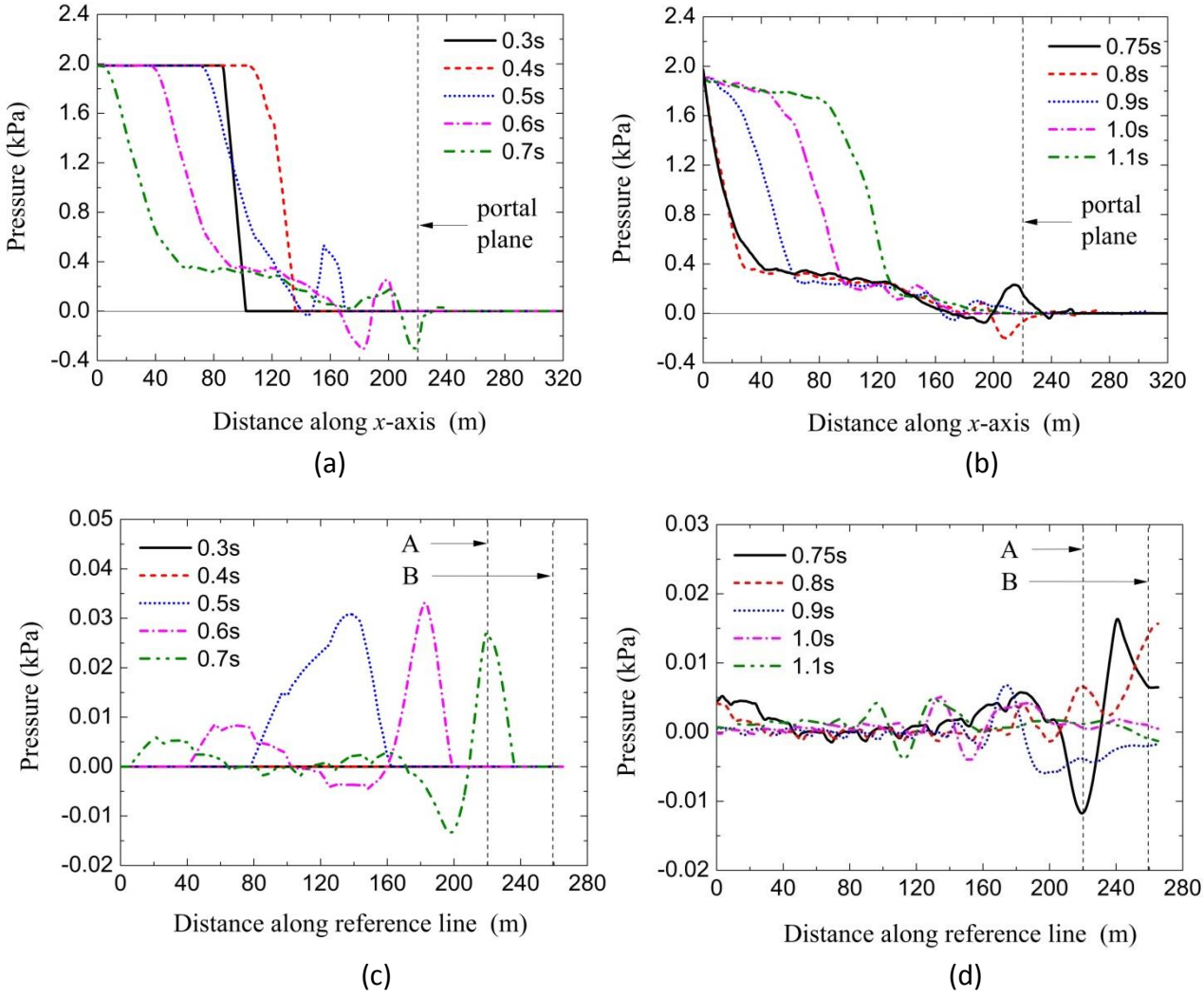

Fig-5 Pressure profiles along the perforated exit region (R_{tun}=5m)
(a) At r=0, until the wavefront reaches the portal plane
(b) Along the reference line, until the wavefront reaches the portal plane
(c) At r=0, after the wavefront toe reaches the portal plane
(d) Along the reference line, after the toe reaches the portal plane

In addition to the radial behaviour associated with each individual slot, there are also strong interactions caused by wave reflections between the various slots. The overall result is much too complex to permit detailed tracking of all of the reflections even in the case of a single step wavefront, let alone in the case of ramped incident wavefronts such as those considered herein. As a consequence, it is necessary to rely on numerical predictions such as those presented in Fig-5. This underlines the importance of the methodology used to ensure that the numerical grid is fit for purpose (as discussed in Section 2.1 above).

Figure-5(b) shows predicted pressure profiles along the reference line as the internal wavefront approaches the exit portal. These highlight an important complication in comparison with the unperforated region, namely that additional MPWs are generated by radiation from every slot. It is essential to allow for these when comparing alternative exit configurations. To illustrate their potential importance, imagine a perforated exit region in which the area of the first hole is very large. In this case, the MPW emitted from it could be comparable to that expected beyond the

portal of an unperforated tunnel. At the other extreme, slots that are very small would have little influence and so would be ineffective in reducing MPW amplitudes. Clearly, a balance must be struck when seeking the optimum configuration. This matter is considered further in Section 5.

Figures-5(c)&(d) show predicted pressure profiles for the period after the toe of the incident wavefront has reached the exit portal plane. In common with the predictions for an unperforated exit region, an MPW propagates beyond the portal and spreads in all directions, including backwards alongside the tunnel. However, the backwards propagation cannot be seen easily because it is superimposed on disturbances originating from the slots at earlier times. This superposition has important consequences for practical design. As already indicated, it complicates the prediction of pressures alongside the tunnel. In addition, however, the pressure fluctuations initiated at the holes spread in all directions, including axially beyond the tunnel portal, thereby superimposing on the pressures emitted from the portal itself. With perforated exit regions therefore, it is not safe to assume that the pressure history at *any* location is dependent solely on the disturbance emitted from the portal plane.

4.1 Influence of incident wavefront characteristics

It is well known that the MPW emitted from a portal of an unperforated exit region is more sensitive to the maximum steepness of the incident wavefront than to its overall amplitude [e.g. Ozawa, et al 1991]. This characteristic can be inferred from Fig-4(c) which shows pressure histories at locations along the reference line up to the point where it meets the tunnel axis beyond the portal (i.e. r=0). It can be seen that the maximum amplitudes of the MPWs are reached at an early stage during the reflection process. That is, the maximum would have occurred even if only the first part of the incident wavefront had existed. This behaviour is a common feature of many acoustic analyses. For example, the amplitudes of pressure disturbances propagating from a point source (e.g. an acoustic monopole) are determined by *rates of change* of mass flow at the source, not by *absolute* rates of flow.

Naturally, the same generic behaviour also influences the outcome alongside slots in perforated exit regions. However, the outcomes at such locations are not determined solely by radiation from a single source. Instead, they may be considered as a superposition of radiation from multiple slots. The only exception to this behaviour is the region close to the first slot. Until the arrival of pressure changes radiated from the second slot, pressure changes in this region will be caused solely by emissions the first slot. The consequences of superpositions are now explored by assessing dependence on the duration, amplitude and steepness of the incident wavefront. These three parameters are inter-dependent (steepness = amplitude ÷ duration), but each is important in its own right.

Figure-6 shows pressure histories at successive locations along the reference line, namely alongside slots 1, 4, 7 & 10 and at r=0 beyond the portal. Three cases are shown. The initial steepness of the incident wavefront is the same in all three cases, namely $(\partial p/\partial t)_0$ = 40 kPa/s. However, the durations - and hence the amplitudes - are different. These are the first three cases listed in Table-2. The continuous lines in the figure denote the base case presented above. The use of the words “Initial states” in the title of the table implies that these conditions apply at the upstream boundary where the wavefront is initiated. However, the wavefronts steepen as they propagate along the tunnel so their steepness on reaching the exit region is somewhat greater than that shown in the table. This effect is stronger for steep wavefronts than for shallow ones.

Beyond the exit portal (at r=0), the MPW amplitudes are almost the same for all three cases, thus almost reproducing the behaviour inferred above from Fig-4(c) for an unperforated exit region. That is, the MPW amplitudes are determined by the steepness of the early part of the arriving wavefront and do not subsequently increase further (because the prescribed steepness does not increase). Alongside the tunnel however, the MPW amplitudes deviate from this behaviour by increasing amounts as the distance from the portal increases. At the upstream locations, the peak amplitudes do not occur at the same instant for all three incident wavefronts, thus showing that account needs to be taken of the duration of the pressure ramp as well as its steepness. Furthermore, even in the cases for which the timings of two maxima are similar, the amplitudes are nevertheless different. These outcomes are a consequence of the phase differences between the pressure disturbances arriving at any particular location from the various slots. It is therefore clear that simple rules such as "proportional to steepness" do not apply at locations influenced by more than one slot.

Table 2 Initial states of incident wavefronts

		Δp[Pa]	Δt[s]	Δp/Δt[kPa/s]
Wavefront 1	$(\partial p/\partial t)_0$	2000	0.05	40
Wavefront 2	$(\partial p/\partial t)_0$	4000	0.1	40
Wavefront 3	$(\partial p/\partial t)_0$	1000	0.025	40
Wavefront 4	$2(\partial p/\partial t)_0$	2000	0.025	80
Wavefront 5	$½(\partial p/\partial t)_0$	2000	0.1	20

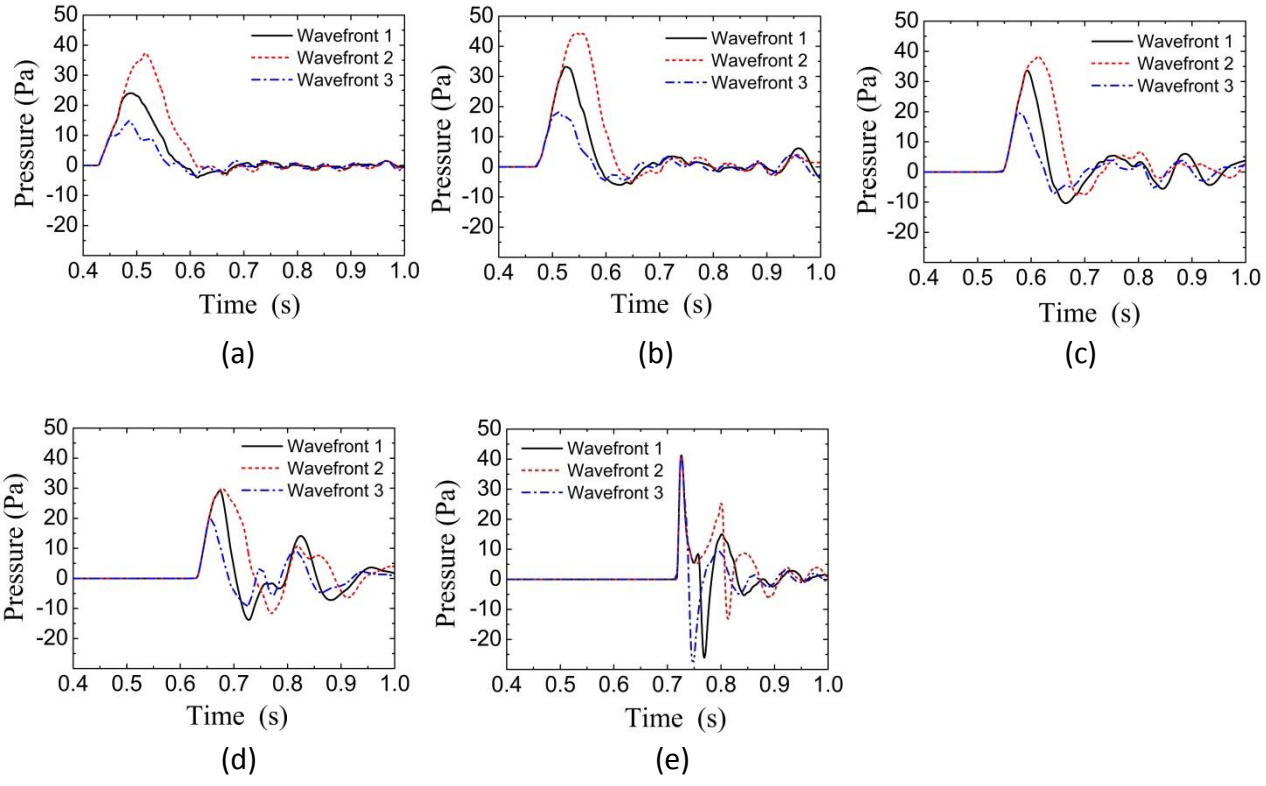

Fig-6 Pressure histories for incident wavefronts of equal initial steepness
(a) Alongside slot-1

(b) Alongside slot-4
(c) Alongside slot-7
(d) Alongside slot-10
(e) At the axis beyond the portal

4.2 Wavefronts with equal amplitude

Figure-7 shows three cases with incident wavefronts of equal amplitude (2 kPa), but different durations - and hence different average steepness. These are cases 1, 4 & 5 in Table-2. The continuous lines denote the case of an incident wavefront with the same initial steepness as the base case (40 kPa/s) and the broken lines show cases with initial steepnesses of twice and half this value.

At all locations, the peak amplitude of the MPW increases with increasing steepness. However, the sensitivity to steepness is not the same at all locations. This can be seen from a cursory glance at the figures and one consequence is that the maximum value does not occur at the same location for all three cases. Beyond the exit portal (at r=0), the maximum *is* approximately proportional to the steepness, as it is for unperforated exit regions. Alongside the tunnel, however, the correlation between the MPW-amplitude and the incident wavefront steepness reduces with increasing distance from the portal. For instance, alongside slot-1, the influence of steepness is much smaller than it is alongside slot-10. Furthermore, the deviation from "proportional to steepness" increases with increasing steepness of the wavefronts. This is seen most easily alongside slots-4 & 7. It can be inferred that, in contrast to an MPW for a simple portal, the *duration* of the incident wavefront ramp does influence the outcome.

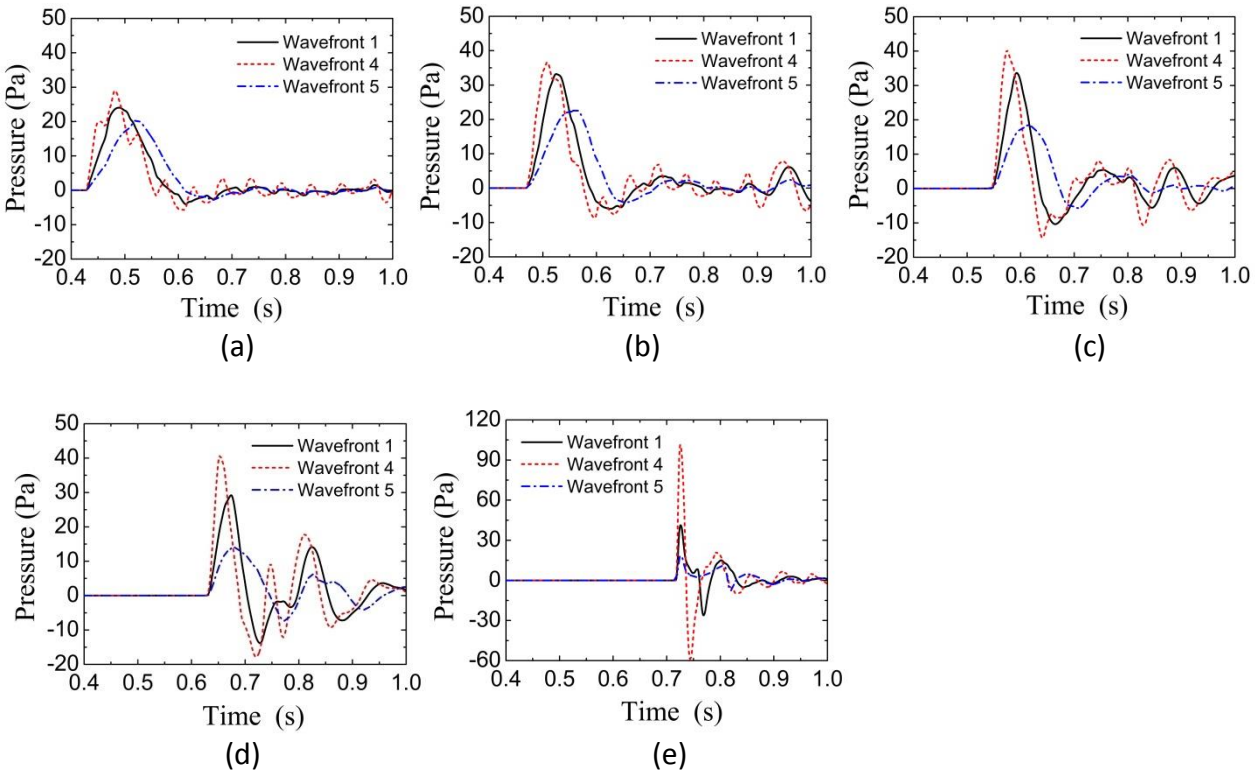

Fig-7 Pressure histories for incident wavefronts of equal amplitude
(a) Alongside slot-1
(b) Alongside slot-4

(c) Alongside slot-7
(d) Alongside slot-10
(e) At the axis beyond the portal

4.3 Wavefronts with equal steepness

Now consider incident wavefronts with identical initial steepness, but different durations – and hence different overall amplitudes. Fig-8 shows how the maximum MPW amplitude varies along the reference line. In Fig-8(a), the initial duration is 0.1 s and in Fig-8(b), it is 0.025 s. The maximum values occur at different times at different locations, but that is of little importance for design purposes.

One important conclusion from the figures is that the overall behaviour is strongly dependent upon the duration of the ramp. This outcome is easily explained even though it contrasts sharply with the unperforated case, for which the duration is unimportant provided that it is sufficiently larger than the R_{tun}/c. The markedly different outcome with a perforated exit region is obtained because of the manner in which pressure fields induced at the various slots superimpose upon one another. The phasing of the superpositions is dependent upon the ratio of the ramp length (duration x wavespeed) and the distance between the slots. That is, for any particular exit region geometry, the duration of the ramp may be loosely regarded as controlling phase effects in the external wave superpositions.

A second conclusion from the figure is that the relative amplitudes of MPWs alongside the tunnel and beyond the portal (characterised by the portions of the graphs between the locations A & B) depend strongly on the duration of the wavefront. This is a somewhat inconvenient property of perforated regions because the designer of a tunnel exit region will not have direct control over the nature of the incident wavefronts that will occur during the lifetime of the tunnel. However, the consequences of the limitation might not be severe because it is not essential to achieve optimum performance for all possible incident wavefronts. If the exit region is optimised for the most severe possible incident wavefront, sub-optimal performance for less severe wavefronts will usually be acceptable. In practice, therefore, the region would be designed for the most severe case and its performance for a representative selection of other cases would then be checked.

An implicit assumption has been made in the preceding paragraph, namely that the geometry of the simulated exit region is close to optimal for the wavefront considered in Fig-8(a), but sub-optimal for the shorter wavefront considered in Fig-8(b). In particular, it is assumed that an increase in the widths of the slots would cause an increase in MPW amplitudes alongside the tunnel, but a decrease in the corresponding amplitudes beyond the portal. This assumption is no more than a simple extrapolation of the original justification for considering the use of perforated exit regions at all. Nevertheless, it has not yet been proven formally and, in any case, the qualitative behaviour needs to be quantified. This is the purpose of the following section.

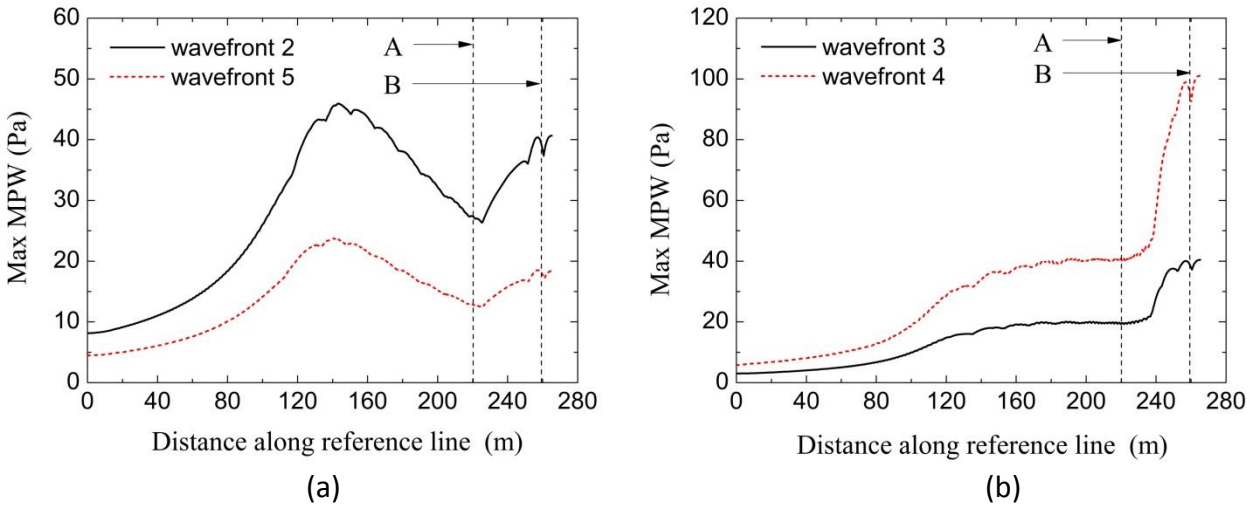

Fig-8 Dependence of the maximum MPW on location along the reference line
(a) Wavefront duration = 0.1 s
(b) Wavefront duration = 0.025 s

4.4 Overall effectiveness of the base case configuration

For engineering purposes, the most important beneficial property of a perforated exit region is its ability to reduce the amplitudes of MPWs. The least desirable aerodynamic consequence is the increase in the number of locations from which MPWs will radiate. Table-3 focuses on the beneficial property. It shows the maximum amplitudes of pressure along the reference line alongside the tunnel and beyond the portal (i.e. between the points "A" and "B" in Fig-2). In all cases, the overall amplitude of the incident wavefront is 2kPa. The rate of change of pressure is varied solely by adjusting the duration of the wavefront (as in Section 4.2). One possible measure of the effectiveness of the perforated region is the proportional reduction that is achieved in the maximum amplitudes of the pressure disturbances. Using this measure and the data in Table-3, the effectiveness of the base case region may be characterised by the proportional reduction shown in the last column of the Table. For this purpose, the relevant MPW amplitude for the perforated exit is taken to be the greater of the values alongside the tunnel and beyond the portal. If account needed to be taken only of the value beyond the portal, the proportional reduction for the case with smallest steepness would increase from 43% to 55%.

In the case of *unperforated* regions, it is well-known that, sufficiently far beyond the portal, the maximum amplitudes of MPWs scale approximately with the steepness of the incident wavefront. Table 3 provides evidence that this approximation applies quite close to the portal even on the axis $y = 0$, notwithstanding the delays implied by the mechanism illustrated in Fig-3(b). To confirm this, it is necessary to allow for steepening of the wavefront as it propagates from the upstream boundary to the portal. The rate of shortening is identical in the three cases shown, but the consequential rates of steepening increase strongly with the initial steepness. By inspection, the maximum MPW amplitude correlates quite closely with the steepness just before the portal. It is not possible to make equivalent comparisons in the case of *perforated* exit regions because local rates of change of pressure are influenced as strongly by reflections propagating upstream as by waves propagating towards the portal.

Table-3 Maximum MPWs at locations along the reference line, Pa

Exit Region	Steepness of 2kPa wavefront (kPa/s)		Maximum MPW alongside tunnel from (0,31) to (220,31)		Maximum MPW beyond portal plane from (220,31) to (245,0)		Proportional reduction
	Upstream	Close to portal	Amplitude Pa	Location (x), m	Amplitude Pa	Location (x,y), m	%
Unperforated	20	22.1	26	220	**42**	245, 0	n/a
	40	50.4	51	220	**95**	245, 0	n/a
	80	140.4	70	220	**257**	245,0	n/a
Perforated	20	n/a	**24**	140.20	19	245, 0	43
	40	n/a	34	166.45	**41**	245, 0	57
	80	n/a	41	206.83	**101**	245,0	61

5 Influence of slot area

So far, a fixed geometry has been assumed and the incident wavefront has been varied. In the remainder of the paper, the wavefront is fixed (identical to the above base case) and the exit region geometry is varied. First, Fig-9 illustrates the influence of the slot width (and hence area) on MPW amplitudes along the reference line. The continuous lines represent the base case geometry considered in Figs-5-7 and the broken lines show predictions using slots with smaller and larger widths.

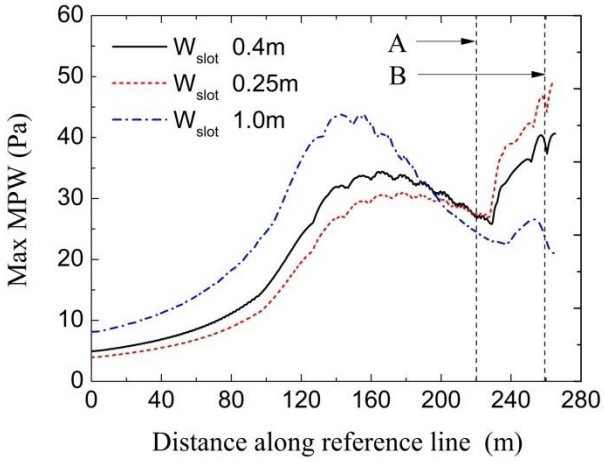

Fig-9 Influence of slot width on the maximum MPW along the reference line.
(Incident wavefront ramp = 2 kPa in 0.05 s = 40 kPa/s)

The figure confirms the behaviour assumed implicitly in the discussion on wavefront duration. That is, for a given wavefront, the greater the slot width, the greater the MPW amplitude alongside the tunnel and the smaller the amplitude beyond the portal. If the design target is the maximum overall amplitude, it may be deduced from the figure that the optimum slot width for the wavefront considered would be slightly greater than the base case value. This is not necessarily the optimum overall value, however. As shown above, that cannot be determined until after assessing the outcomes for a representative range of incident wavefronts. Also, the most appropriate target design is not necessarily a balance between the maxima alongside the tunnel and beyond the portal. Account must also be taken of the purposes for which the region

outside the tunnel is used. Furthermore, the particular reference line chosen for the purposes of this paper will not be the most suitable reference in all particular applications. Nevertheless, figures such as Fig-9 are highly informative for development purposes and similar figures will be equally valuable in practical design.

6 Influence of distribution of slot area

In a strict interpretation of the axi-symmetric geometry chosen herein for analytical convenience, the base case geometry has ten constant-width slots at axial intervals equal to the diameter of the semi-circular tunnel cross section. Numerically, each slot is of uniform width and extends around the whole of the tunnel circumference. However, it is intuitively obvious that, physically, the particular geometry of individual slots will be of secondary importance in comparison with the axial distribution of the pressure relief that the slots provide. Thus, for instance, the simulations will be broadly valid for ten discrete holes of any plausible shape at the same axial locations, provided that their areas are equal to those of the assumed slots. In a detailed design for any particular application, it might be considered worthwhile to undertake specific simulations with full 3-D geometry, but that would have little practical benefit for the generic purposes of this paper. Instead, attention now focuses on the *axial* distribution of the pressure relief slots.

Figure-10 compares the base case solution with the corresponding solution for an alternative configuration with the same total slot area provided by half the number of slots. That is, instead of ten 0.4 m wide slots at 10 m intervals, there are five 0.8 m wide slots at 20 m intervals. These are in the same locations as slots 1, 3, 5, 7 and 9 in the base case configuration. By inspection, if the target is to achieve a balance between the maximum MPW amplitudes alongside the tunnel and beyond the portal, the coarser distribution of slots is less effective than the finer distribution. However, using the evidence illustrated in Fig-9, a balance could be achieved in both cases by a small increase in the slot widths and the outcomes of the two cases would then be similar. As a consequence, it may be concluded that the potential effectiveness of a uniformly perforated exit region is influenced less by the discreteness of slot locations than by their total area.

Another difference between the two cases shown in Fig-10 is in the region upstream of the first slot (i.e. $0 < x < 120$ m). In this region, the MPW amplitude is strongly dependent on the area of slot-1. It is concluded above that there will be an upper limit to the acceptable size of this slot. This figure shows that the limiting value will be influenced by the distance between slot-1 and subsequent slots. In a practical design, this effect will need to be quantified for a range of plausible incident wavefronts (Fig-10 applies only to the base-case wavefront).

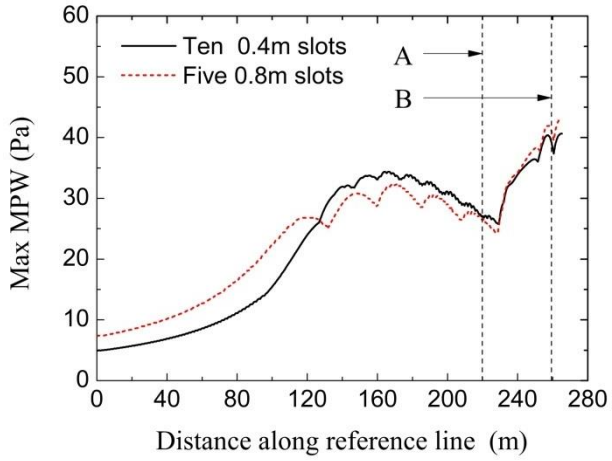

Fig-10 Influence of slot area distribution on maximum MPW along the reference line.

7 Influence of slot height

In all of the preceding examples, the slots are imagined to be holes in the wall of a purpose-built extension region. The wall thickness is chosen as 1 m. This configuration would facilitate considerable freedom in the choice of sizes, shapes and locations of the holes providing pressure relief. However, since a good outcome is possible with a small number of holes, it is natural to explore whether some or all of the relief could be provided by short shafts within the tunnel itself instead. This would have the important practical benefit of avoiding the need for an extension region – or, at least, reducing the required length thereof. This possibility is assessed in Fig-11, in which the 5-hole case presented in Fig-10 is compared with a configuration that is identical except for an increased slot height (shaft length).

Alongside the tunnel, the reference lines used for the two cases shown in Fig-11 are at the same overall radius, namely 31 m. Noting that the inner radius of the tunnel is 5m, this implies a distance of 25 m from the outer surface of its 1 m thick wall, but only 21 m from the outlets of the 5 m long "shafts". In both cases, however, the lines beyond the portal are 25 m from the portal plane. This choice of reference line is convenient numerically and it avoids complications that would arise if different radii were chosen for the two cases. It has little implication for practical purposes because reference lines might not be used at all in a practical detailed design. Such designs must satisfy acceptability criteria at specific locations (e.g. at houses or roads), not at generic reference lines.

By inspection, the increase in slot height causes a reduction in amplitudes alongside the tunnel (even though the outlets are closer to the reference line) and a corresponding increase beyond the portal. Once again, using the evidence in Fig-9, it is clear that the resulting imbalance could be eliminated by increasing the areas of the slots/shafts. It seems likely that the common amplitude of the two maxima would be slightly greater than that with the 1 m thick wall, but this is not a strong effect. Accordingly, there is clearly scope for using shafts to exploit visual and financial advantages that could arise from consequential reductions in the required lengths of extended exit regions.

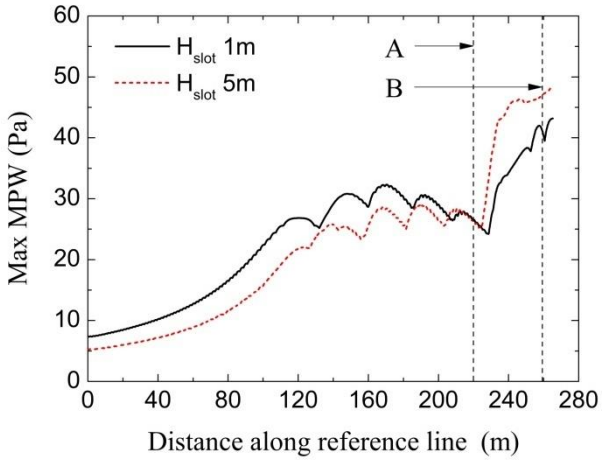

Fig-11 Influence of slot height on maximum MPW along the reference line.

8 Conclusions

The use of long, perforated exit regions to reduce the amplitudes of pressure disturbances emitted from railway tunnels has been investigated using CFD analysis for axi-symmetric geometries that are approximately representative of tunnels emerging into open ground. The investigation has assessed the influence of (a) the amplitude and steepness of incident wavefronts arriving along the tunnel and (b) the geometrical arrangement of slots along the perforated region. The principal conclusions may be summarised as follows:

1. For simple tunnel portals, the amplitudes of the emitted waves are strongly dependent upon the steepness of wavefronts approaching the exit from upstream. In short tunnels, suitable counter-measures can prevent the development of unacceptably large steepness. In long tunnels, however, wavefront steepening effects can greatly reduce the effectiveness of such measures. Exit portal measures can then be attractive alternatives.

2. Perforated exit regions have a dispersive influence on wavefronts reaching the end of a tunnel. By enabling pressure relief before a wavefront reaches the exit portal, they reduce the amplitudes of disturbances emitted directly from the portal. However, this is achieved at the expense of causing disturbances alongside the regions. The areas of the slots need to be sufficiently large to provide adequate relief at the portal, but not so great that the problem is simply transferred elsewhere.

3. It has been shown that the effectiveness of any particular perforated exit region is strongly dependent upon the amplitude and duration of an incident wavefront, not only on its steepness. As a consequence, the optimum design of such regions will be application-specific and, in each case, it will be necessary to identify the most design-critical wavefront. Nevertheless, the generic simulations presented herein provide indicative guidance on required slot sizes.

4. It has been shown that the relative amplitudes of the maximum pressures alongside and beyond a perforated exit region depend primarily on the overall cross-sectional area of all holes in its wall. This parameter is more important than either the number of holes or their lengths.

In any particular application, the design objective will be to minimise disturbances at site-specific locations. This will influence the required balance between pressure amplitudes alongside the tunnel and beyond its portal. As a consequence, it will influence the optimum area of pressure relief holes. Other practical considerations will include matters such as visual impact and financial cost. As a consequence, the particular optima identified herein will not be universally appropriate. Nevertheless, the overall methodology provides a robust guide to the behavioural trends that will be exhibited in each specific case.

In principle, the solution method presented in this paper could be used for practical assessments of real tunnels. The only strong change would be the replacement of the assumed pressure history at the upstream tunnel boundary by actual (expected or measured) pressure histories. Realistically, however, 2-D and 3-D analyses are too resource-intensive for comparing large numbers of alternative designs. In the near future, therefore, it is therefore likely that practical design would utilise the generic behaviour from papers such as this and that the 2-D or 3-D methodology would be reserved for assessing the suitability of particular proposed geometries to a representative selection of incident wavefronts.

Acknowledgements

The authors are grateful to the following bodies that provided financial support for the project: (i) China Scholarship Council, (ii) National Natural Science Foundation of China (Grant No. U1334201 and (iii) UK Engineering and Physical Sciences Research Council (Grant No. EP/G069441/1).

REFERENCES

Aoki,T, Vardy,AE & Brown,JMB (1999) Passive alleviation of micro-pressure waves from tunnel portals, *Journal of Sound and Vibration*, **220**(5), 921-940.

ANSYS FLUENT Manual, Release 14.0, 2011.

Degen,KG, Gerbig,Ch, & Onnich, H (2008) Acoustic Assessment of Micro-pressure Waves Radiating from Tunnel Exits of DB High-Speed Lines. *Noise and Vibration Mitigation for Rail Transportation Systems, Notes on Numerical Fluid Mechanics and Multidisciplinary Design*, **99**, 48-55.

Fukuda,T, Ozawa,S & Iida,M (2006) Distortion of Compression Wave Propagating through Very Long Tunnel with Slab Tracks, *JSME International Journal, series B*, **49**(4), 51-57.

Gerbig,Ch & Degen,KG (2012) Acoustic assessment of micro-pressure wave emissions from high-speed railway tunnels, *Noise and Vibration Mitigation for Rail Transportation Systems, Notes on Numerical Fluid Mechanics and Multidisciplinary Design*, **118**, 389-396.

Hieke ,M, Gerbig,Ch, Tielkes ,T & Degen,KG (2011) Assessment of micro-pressure wave emissions from high-speed railway tunnels, *Proc 9th World Congress on Railway Research: Challenge B: An environmentally friendly railway , Lille, France, 22-26 May 2011, 9pp*.

Kim,H, Kweon,YH & Aoki,T (2004) A new technique for the control of a weak shock discharged from a tube, *Journal of Mechanical Engineering Science, Part C*, **218**(4), 377-387.

LeVeque, RJ (2002) Finite Volume Methods for Hyperbolic Problems, Cambridge University Press, 558pp.

Mashimo,S, Nakatsu,E & Aoki,T (1997) Attenuation and Distortion of a Compression Wave Propagating in a High-Speed Railway Tunnel, *JSME International Journal, series B*, **40**(1), 51-57.

Matsubayashi,K, Brown,JMB & Vardy,AE (2000) Sonic booms - do I have a problem?, *Proc 10th int symp on the Aerodynamics and Ventilation of Vehicle Tunnels, Boston, USA, 1-3 Nov 2000,* BHR Group, 185-202.

Matsubayashi,K, Kosaka,T & Kitamura,T (2004) Reduction of micro-pressure wave by active control of propagating compression wave in high speed tunnel, *Journal of Low Frequency Noise, Vibration and Active Control*, **23**(4), 259-270.

Miyachi,T, Fukuda,T & Iida,M (2008) Distortion of Compression Wave Propagating through Shinkansen Tunnel, Noise and Vibration Mitigation, *Notes on Numerical Fluid Mechanics*, **99**, 9-18.

Ofengeim,DKh, Drikakis,D (1997) Simulation of blast wave propagation over a cylinder, *Shock Waves Journal*, **7**, 305-317.

Ozawa,S & Maeda,T (1988) Tunnel entrance hoods for reduction of micro-pressure wave, *Quarterly Report of RTRI*, **29**(3), 134-139.

Ozawa,S, Maeda,T, Matsumura,T, Uchida,K, Kajiyama,H & Tanemoto,K (1991) Counter-measures to reduce micro-pressure waves radiating from exits of Shinkansen tunnels, *Proc 7th int symp on Aerodynamics and Ventilation of Vehicle Tunnels, Brighton, UK, 27-29 Nov 1991*, BHR Group, 253-266.

Ozawa, S (1992) Present situation and future outlook of aerodynamic and aeroacoustic problem of high speed trains, *Quarterly Report of RTRI*, **33**(1), 47-56.

Ozawa,S, Maeda,T, Matsumura,T & Uchida,K (1993) Micro-pressure waves radiating from exits of Shinkansen tunnels, *Quarterly Report of RTRI*, **34**(2), 134-140.

Raghunathan,SR. Kim,HD & Setoguchi,T (2002) Aerodynamics of high-speed railway train, *Progress in Aerospace Sciences*, **38**, 469-514.

Ravn,S & Reinke,P (2006) Tunnel aerodynamics of the magnetic levitation high-speed link in Munich(MAGLEV) – Consequences for pressure comfort, micro pressure waves, traction power and pressure loads, *Tunnel Management International Journal*, **9**(1),1-10.

Sockel,H & Pesave,P (2006) The reduction of micro pressure waves by baffles, *Proc 9th int symp on Aerodynamics and Ventilation of Vehicle Tunnels, Portoroz, Slovenia, 11-13 July 2006*, BHR Group, 804-817.

Toro EF (2001) Shock-Capturing Methods for Free-Surface Shallow Flows. Wiley and Sons Ltd: Chichester.

Vardy,AE (2008) Generation and alleviation of sonic booms from rail tunnels, *Engineering & Computational Mechanics, Proc ICE*, **161**(EM3), 107-119.

Wang,H, Vardy,AE & Pokrajac,D (2015) Pressure radiation from a perforated duct exit region, *Journal of Sound and Vibration*, http://dx.doi.org/10.1016/j.jsv.2015.03.040i

Zoltak,J & Drikakis,D (1998) Hybrid upwind methods for the simulation of unsteady shock-wave diffraction over a cylinder, *Computer Methods in Applied Mechanics and Engineering*, **162**, 165-185.